Biophysical Journal Volume 105 July 2013 211–221

Mode-Specific Reorganization Energies and Ultrafast Solvation Dynamics of Tryptophan from Raman Line-Shape Analysis

Erix A. Milán-Garcés,[†] Shreyas Kaptan,[†] and Mrinalini Puranik[‡*]

[†]National Centre for Biological Sciences, Tata Institute of Fundamental Research, Bangalore, India; and [‡]Indian Institute of Science Education and Research, Pune, India

ABSTRACT Tryptophan is widely used as an intrinsic fluorophore for studies of protein structure and dynamics. Its fluorescence is known to have two decay components with lifetimes of 0.5 and 3.1 ns. In this work we measure the ultrafast dynamics of Tryptophan at <100 fs through measurements and modeling of the Raman excitation profiles with time-dependent wave packet propagation theory. We use a Brownian oscillator model to simulate the water-tryptophan interaction. Upon photoexcitation to the higher singlet electronic state (B_b) the structure of tryptophan is distorted to an overall expansion of the pyrrole and benzene rings. The total reorganization energy for Trp in water is estimated to be 2169 cm^{-1} with a 1230 cm^{-1} contribution from the inertial response of water. The value of reorganization energy of water corresponding to the fast response is found to be higher than that obtained upon excitation to the L_a state by previous studies that used computational simulations. The long-time dynamics of Trp manifests as a conformational heterogeneity at shorter times and contributes to inhomogeneous broadening of the Raman profiles (315 cm^{-1}).

INTRODUCTION

Tryptophan (Trp) is widely used as an intrinsic probe of protein structure and dynamics in several spectroscopic techniques (1–4). It is especially popular in fluorescence-based spectroscopies because of the sensitivity of its emission spectra to changes in the local environment. The solvation dynamics of Trp in water and in proteins has been examined by several theoretical and experimental studies at timescales ranging from femtoseconds to picoseconds (5–14). Computational studies have predicted a response at <50 fs in water (6,7). However, no direct experimental evidence has been possible at this short timescale. In the following, we determine the short-time (<100 fs) dynamics of Trp in water from Raman intensity analysis.

Photophysics of Trp has been extensively studied. The absorption spectrum and molecular structure of Trp are shown in Fig. 1, *a* and *b*. Trp has two π-π^* electronic transitions, L_a and L_b, at 270 and 280 nm from which fluorescence emission occurs. L_a is more sensitive to solvent polarity because of a higher permanent dipole moment. A pair of stronger,π-π^* transitions to the B_a and B_b excited states, appear around 197 and 220 nm, respectively (15). Raman excitation within the B_b band selectively enhances bands of Trp over those of other amino acids, making it a useful probe in vibrational resonance Raman (RR) spectroscopy as well (16,17).

Raman shifts of Trp are altered in response to hydrogen bonding, stacking, and ionic interactions with amino acids and ligands in proteins (18,19). In addition to the band positions, intensities of the RR spectra contain information about the nature of the local environment such as hydrophobicity. Additionally, the line-shape of the Raman excitation profile (REP), i.e., excitation wavelength dependence of the Raman spectrum, contains information on the dynamical response of the environment through line broadening.

Intensities of Raman bands at a given excitation wavelength are determined by properties of the vibronic potential energy surface (PES) in the Franck-Condon region of resonant vibronic excited state. Position of the minimum of the vibrational PES is determined by the structure of the excited state compared to that in the ground state. Slope of the excited state PES determines initial structural dynamics of the molecule upon photoexcitation. Because the ground and excited vibrational PESs are coupled through the resonant electronic excitation, REP of the ground state contains information on the excited state PES. Through simulations of the REP and a thorough theoretical analysis, it is possible to extract the structural changes in a molecule within a few femtoseconds after photoexcitation. Lineshape of the REP (and the PES) are also influenced by dynamics of the surrounding solvent on the ultrafast timescale (homogeneous broadening) as well as by the presence of static microenvironments of the chromophore (inhomogeneous broadening). Thus, deconvolution of the REP into homogeneous and inhomogeneous effects provides an insight into the solvent (or protein) dynamics after photoexcitation of Trp. A valuable parameter obtained uniquely from Raman intensity analysis is a partitioning of the total reorganization energy into its intramolecular and intermolecular (solvent) components, improving our understanding of the interactions of molecules with the environment on the femtosecond timescale (20–23).

REP within the B_b band of Trp has been measured previously (24–27). These measurements differed in the vibronic structure observed in the REP, which was ascribed to occurrence of saturation phenomena near the maximum of the B_b

Submitted December 20, 2012, and accepted for publication April 22, 2013.

*Correspondence: mrinalini@iiserpune.ac.in

Editor: Catherine Royer.

0006-3495/13/07/0211/11 $2.00

http://dx.doi.org/10.1016/j.bpj.2013.04.044

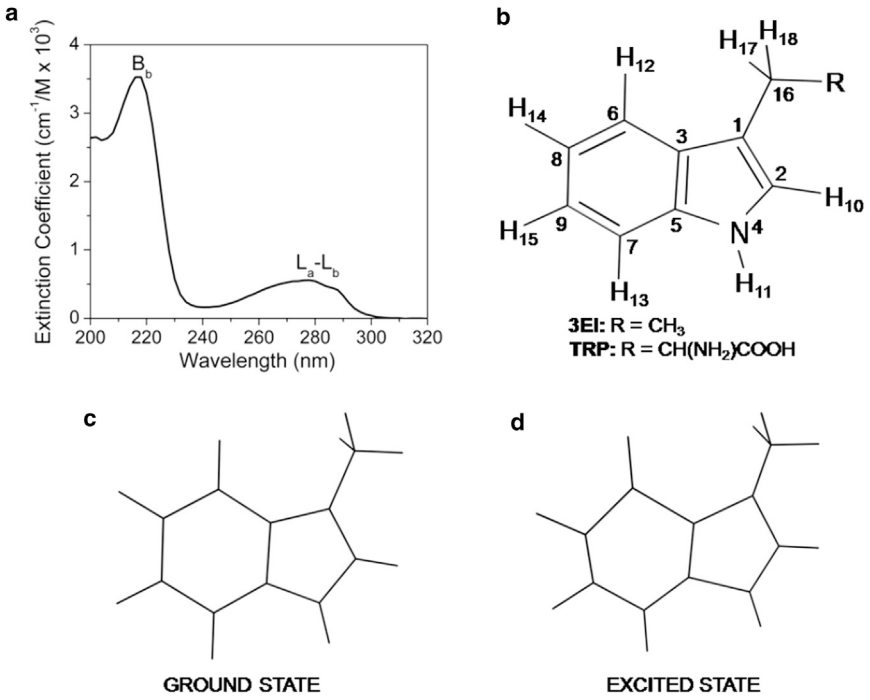

FIGURE 1 (*a*) Absorption spectrum of Trp in water. (*b*) Structure of tryptophan and 3EI that was used to model tryptophan in DFT (B3LYP/6-31G**) calculations. Atom numbering used in the calculations and in discussion in the text are shown. (*c*) Energy-minimized structure of the ground state of 3EI. (*d*) Schematic representation of the structural distortion in the indole ring upon excitation to the B_b state of Trp determined from simulations of resonance Raman intensities. Displayed bond lengths have been scaled to 3× the actual displacement for visual clarity. Changes in the internal coordinates of the ground state upon photoexcitation were computed from the displacements between the ground and excited state potential energy surfaces along each normal mode. The displacements used correspond to the best fit to the experimental REP.

absorption band and throughput characteristics of the monochromators employed. These measurements were carried out with the low-repetition rate, high-peak power lasers available at that time. A third measurement of the REP of Trp (207–250 nm) was made by Sweeney and Asher (26), which showed red-shifted REP with λ_{max}~224 nm. The latter work employed a sum-over-states methodology to simulate the REP. The model included interference between the B_b and B_a transitions and homogeneous effects. However, the simulations failed to reproduce the red-shift in the REP. Apart from the experimental studies summarized above, several computational studies to model tryptophan REP have also been made using sum-over-states method (28) and time-dependent Density Functional Theory (TDDFT) (29–31).

In the absence of a consensus on the experimental REP reported in the literature, and in view of the recent advances in UV resonance Raman (UVRR) spectroscopy of biological molecules, we have made meticulous new measurements of the REP of Trp within the B_b band using a high-repetition rate laser that minimizes photodamage. All the experimental and computational studies summarized above have focused on the structure of the excited state, B_b. In this article, we determine the excited state structure and also demonstrate the utility of Trp as a vibrational probe of the short-time local solvation dynamics in water.

We use time-dependent wave propagation formulation to simulate the experimental REP and extract the short time excited-state structural dynamics (21,32). The Trp-water interaction is modeled using the Mukamel model (21,33,34). From these simulations, we determined:

1. Excited state structure in terms of the change in internal coordinates of the ground state;
2. Partitioning of the internal reorganization energy into vibrational normal modes; and
3. Relative contributions of static (inhomogeneous) and dynamic (homogeneous) components of the Trp-water interactions.

We expect that the combination of rigorous Raman intensity analysis that we report here, with a detailed interpretation of the environment-induced shifts in the Raman spectrum, can provide a more complete picture of the photodynamics of Trp. This analysis can be extended to Trp moieties within proteins to understand the local protein dynamics and protein heterogeneity at short timescales.

MATERIALS AND METHODS

Experimental methods

UVRR spectra of Trp were obtained with Raman excitation between 210 and 230 nm using a tunable Ti:sapphire laser (Photonics Industries, Bohemia, NY). Excitation light source is the fourth harmonic of an Nd:YLF laser pumped Ti:sapphire laser (Photonics Industries). For the second and fourth harmonic generation the fundamental output was passed through lithium borate crystals. Raman samples contained a solution of 1.0 mM Trp in 0.1 M of sodium phosphate buffer at pH 7. The solution also contains 1.0 M of sodium perchlorate as the internal intensity standard. L-tryptophan was purchased from Sigma Aldrich (St. Louis, MO) and used as received.

In all the experiments the typical incident laser power was 0.6 mW. The samples were kept in a rotating NMR tube. The scattered light was collected with a 135° backscattering geometry and detected on a charge-coupled device camera with 1024 × 256 pixels after dispersal by a 1250M monochromator (SPEX Industries, Edison, NJ) with 3600 grooves/mm and entrance

slit of 300 μm. Raman spectra were recorded during 5 min of total accumulation time. For each excitation wavelength the final spectrum was obtained by averaging the recorded spectra of three freshly prepared samples. Spectra at each wavelength were normalized to the intensity of the 932 cm^{-1} band of sodium perchlorate. Bands were fitted using Lorentzian functions.

The position and width of each band was kept constant for the spectra at all the excitation wavelengths. Integrity of the sample was checked by comparing the spectrum at the beginning and at the end of each scan and ensuring that the spectra overlapped. For the depolarization ratio measurement of the Raman bands, the scattered light was passed throughout a Glan-laser α-BBO polarizer (ThorLabs, Newton, NJ) placed in front of the slit. To compensate for the polarization dependence of the spectrometer, a scrambler was placed between the polarizer and the spectrometer. The Raman depolarization ratio is defined as

$$\rho = \frac{I_{\perp}}{I_{II}},$$

where $I_{\perp}$ ($I_{||}$) is the intensity collected perpendicular (parallel) to the polarization direction of the incident light. The reliability of the depolarization measurement was verified by measuring the depolarization ratio of the Raman bands of acetonitrile, sodium perchlorate, and sodium nitrate (see Table S1 of the Supporting Material). The values of the depolarization ratio of the solvent were close to those measured previously by DeVito et al. (35).

The absolute Raman cross-sections of each band of Trp was determined from the known Raman cross-sections of the sodium perchlorate (36) using the formula (37)

$$\sigma_N = \frac{8\pi}{3}\left(\frac{1+2\rho}{1+\rho}\right)_N\left(\frac{I_N}{I_S}\right)\left(\frac{C_S}{C_N}\right)\left(\frac{\partial\sigma_S}{\partial\Omega}\right)_{II+\perp}\frac{S(\lambda_S)}{S(\lambda_N)}K(\lambda_N,\lambda_S), \quad (1)$$

where the intensities of the band corresponding to the Nth mode (I_N) and the internal standard (I_S) are determined from measuring areas under the curve for corresponding bands. C_N and C_S are concentrations of the sample (Trp) and internal standard.

$$\left(\frac{\partial\sigma_S}{\partial\Omega}\right)_{II+\perp}$$

is the total differential cross-section of the internal standard. The value ρ is the depolarization ratio of the Raman band of the solute. The depolarization ratios of all bands were close to one-third except for the band at 1625 cm^{-1} (see Table S2). The depolarized and polarized spectra of Trp are shown in Fig. S1 in the Supporting Material. In the case of very low intensity bands, it was difficult to determine the depolarization ratio because of the low signal of the depolarized spectrum. Thus, we assumed as an approximation that the depolarization ratios for these bands are also one-third. $S(\lambda)$ is the spectral sensitivity of the spectrometer and the detector determined by

$$S(\lambda) = \frac{D(\lambda)}{T(\lambda)},$$

where $D(\lambda)$ is the spectrum from a calibrated D_2O lamp (Ocean Optics, Dunedin, FL) recorded at the same grating position as the actual spectrum for each excitation wavelength, and $T(\lambda)$ is the calibrated output of the lamp. Fig. S2 shows the $S(\lambda)$ used to correct the spectrum obtained at 229-nm excitation wavelength.

The factor $K(\lambda_N\lambda_S)$ is introduced to correct for self-absorption of the sample and is computed as (27)

$$K(\lambda_N,\lambda_S) = \frac{\varepsilon_N\chi+\varepsilon_0}{\varepsilon_S\chi+\varepsilon_0},$$

where ε_N and ε_S are the extinction coefficients at the wavelength position of the Raman band of sample and internal standard, respectively. The value ε_0 is the extinction coefficient at the excitation wavelength,

$$\chi = \sin\left[\cos^{-1}\left(\frac{n_1}{n_2}\cos\varphi\right)\right],$$

where n_1 and n_2 are the values of the refractive index corresponding to the air and the sample solution, assuming here to be 1.0 and 1.33, respectively. The value $\varphi = 45^\circ$ is the angle between the excitation light and the tube. To minimize artifacts due to self-absorption of the sample, backscattering geometry was used for collection of the Raman signal.

Absorption spectrum of Trp was measured with a U2010 spectrophotometer (Hitachi High Technologies America, Schaumburg, IL). Concentration of Trp solution was 30 μM. The absorption spectrum was deconvolved into two Gaussians components to determine the contribution from the B_b band that is used in our simulations.

Computational methods—Raman intensity analysis

Experimental Raman and absorption cross-sections were simulated using time-dependent wave packet propagation theory. Simplified expressions of the Raman and absorption cross-sections can be obtained within the harmonic approximation by assuming equal vibrational frequencies in the ground and excited electronic state (34,38,39):

Raman cross-section

$$\sigma_{0\to1}(E_L) = \frac{8\pi^4E_S^3E_LM^4}{9\hbar^6c^4\theta(2\pi)^{1/2}}\int_0^\infty dE\,\exp\left[-\frac{(E-E_0)^2}{2\theta^2}\right] \times\left|\int_0^\infty\exp\left[\frac{i(E_L-E_0)t}{\hbar}-g_{solv}(t)\right]\frac{\Delta_k}{\sqrt{2}}(\exp(-i\omega_k t)-1) \times\prod_{j=1}^{N}\exp\left\{-\frac{\Delta_j^2}{2}\left[1-\exp(-i\omega_j t)\right]\right\}dt\right|^2, \quad (2)$$

Absorption cross-section

$$\sigma_A(E_L) = \frac{4\pi^4E_LM^2}{6\hbar^2nc\,\theta(2\pi)^{1/2}}\int_0^\infty dE\,\exp\left[-\frac{(E-E_0)^2}{2\theta^2}\right] \times\int_{-\infty}^{\infty}\exp\left[\frac{i(E_L-E_0)t}{\hbar}-g_{solv}(t)\right] \times\prod_{j=1}^{N}\exp\left\{-\frac{\Delta_j^2}{2}\left[1-\exp(-i\omega_j t)\right]\right\}dt, \quad (3)$$

where n is the refractive index, M is the transition dipole moment strength, and ω_j is the frequency of the jth normal mode; E_S and E_L are the incident and scattered photon energies; E_0 is the zero-zero transition energy; θ is the static inhomogeneous broadening linewidth; and Δ_j values are the dimensionless displacements in the equilibrium position of the ground and excited

state potential energy surface along the *j*th normal mode. Δ_k and ω_k are the dimensionless displacements and the frequency of the *k*th mode, which undergoes a $0 \rightarrow 1$ transition while the other modes are in the ground state, and g_{solv} is the solvent-dephasing function. A general expression for g_{solv} using the overdamped Brownian oscillator model (33,34) has been used that includes the solvent reorganization energy (λ_S) and the inverse of the solvent correlation time ($\Lambda = 1/2\pi c\tau$).

Solvent-dephasing function

Using the overdamped Brownian oscillator model (33,34,40,41), the following expressions were obtained as

$$g_{solv}(t) = g'(t) + i\, g''(t), \tag{4}$$

where

$$g'(t) = \frac{\lambda_S}{\Lambda}\cot\left(\frac{\hbar\Lambda}{2k_BT}\right)[\exp(-\Lambda t) + \Lambda t - 1] + \left(\frac{4\lambda_S\Lambda\, k_BT}{\hbar}\right)\sum_{m=1}^{\infty}\frac{\exp(-\nu_m t) + \nu_m t - 1}{\nu_m\left(\nu_m^2 - \Lambda^2\right)}, \tag{5}$$

$$g''(t) = -\frac{\lambda_S}{\Lambda}[\exp(-\Lambda t) + \Lambda t - 1], \tag{6}$$

and

$$\nu_m = \frac{2\pi\, mk_BT}{\hbar} \tag{7}$$

are the Matsubara frequencies and *m* is a positive integer.

Internal reorganization energy and coordinates

The total internal reorganization energy is determined by the expression

$$\lambda_{int} = \sum_{j=1}^{3N-6}\frac{\left(\Delta_j^2\hbar\omega_j\right)}{2}, \tag{8}$$

where ω_j is the mode frequency in the ground and excited state and Δ_j is the corresponding dimensionless displacement.

Changes along the internal coordinates are determined from the best-fit dimensionless displacements (23,42,43) using the expression

$$\delta_i = 5.8065\sum_j A_{ji}\,\omega_j^{-1/2}\,\Delta_j. \tag{9}$$

A_{ji} values are the elements of the pseudo-inverse of the matrix *S* that transform from internal coordinates to normal mode coordinates. The value ω_j is the frequency of the *j*th normal mode. The matrix *S* was obtained from the frequency calculation using the software GAUSSIAN03W.

The initial relative deltas were obtained from the intensity of the band relative to that of the 1556 cm^{-1} band in the spectrum recorded at 225.1 nm (assuming, $I \propto \Delta^2$) (38,44). Initial estimates of the other parameters were taken from previous studies and from the position and intensity of absorption and REP. The guess transition dipole moment strength (0.95 Å) and the zero-zero transition energy (44,440 cm^{-1}) were taken from Gaff et al. (30). They used TDDFT calculations to show that the major contribution to the B_b electronic transitions of 3MI (3-methylindole) comes from the transition MO35 (HOMO) → MO37 (29). The water relaxation time (30 fs) was taken from Jimenez et al. (45) obtained from the MPTS (8-methoxypyrene-1,3,6-trisulfonate) solvation dynamics of water measured by using photon echo spectroscopy. The values were then iteratively optimized by using a self-consistent procedure to fit the REP and absorption spectrum. The quality of the fit was initially determined by visual inspection. Finally, these values were then used as input of an automatic optimization procedure using the lsqcurvefit.m routine of MATLAB (The MathWorks, Natick, MA) to get the final values of the parameters. Variations in the parameters were constrained to within 10% of the input values during the automatic optimization.

DFT calculations

Trp is modeled using its reduced analog 3EI (3-ethylindole). The solvent environment around the amino acid was modeled using explicit solvation model. In the explicit solvent model, the 3EI geometry was optimized with a single water molecule in hydrogen bond contact with N–H position (see Fig. S3). The model was combined with the IEFPCM algorithm model to simulate the dielectric environment of bulk water. The structure was optimized using the software GAUSSIAN03W (46). The optimization was done with a completely relaxed geometry using the DFT method. Specifically, the Becke three-parameter method (47) by Lee et al. (48) (known collectively here as B3LYP) was used with 6-31G** Gaussian basis set.

RESULTS AND DISCUSSION

A UVRR spectrum of Trp obtained with Raman excitation of wavelength 229 nm is shown in Fig. 2. Between parentheses are the designations of the Trp bands from Takeuchi and Harada (49). Comparison of the band positions with previous reports shows agreement within experimental error (25,26). Variation in the Raman spectrum as the excitation wavelength is tuned across the electronic absorption spectrum can be seen in Fig. 3. Intensity of each spectrum is normalized to the intensity of the band of sodium perchlorate at 932 cm^{-1} that was used as an internal intensity standard. Overall, the Raman cross-section of Trp peaks at ~223 nm. There is no appreciable change in the band positions with change in Raman excitation wavelength.

Experimental REP made with normalized intensities, simulated REP, and the B_b band of absorption spectrum of Trp are shown in Figs. 4 and 5, and the parameters corresponding to the best fit of simulated REP to the experimental data are tabulated in Table 1. Overall, an excellent agreement is found between the experimental and simulated REPs. Table 2 lists values for the dimensionless displacement, Δ, and the internal reorganization energies for major normal modes corresponding to the best fit to the experimental REP. Additional details are provided in Table S2.

The W7 doublet of Trp occurs because of Fermi resonance between a fundamental and one or two combinations of out-of-plane vibrations (~600 cm^{-1} + ~745 cm^{-1} and ~420 cm^{-1} + ~920 cm^{-1}) (49–51). The lower frequency region of the spectrum at 225 nm (see Fig. S4) shows that there are no intense bands, and thus the fundamental modes corresponding to the combination bands in the Fermi doublet are absent. These combination bands therefore do

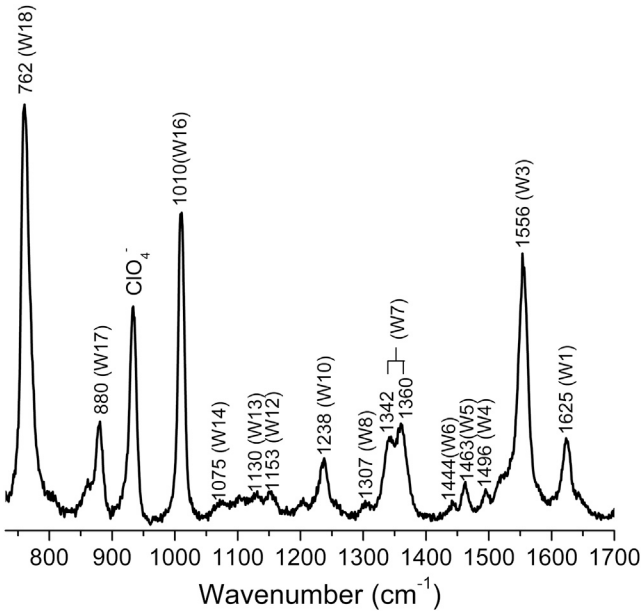

FIGURE 2 UVRR spectrum of tryptophan obtained with excitation wavelength of 229 nm. The band at 932 cm^{-1} corresponds to the internal standard sodium perchlorate.

not contribute to the overall Raman analysis in this model. We have included the higher frequency component (fundamental band) of the Fermi doublet in the global fit to the REP (51).

A previous measurement of Trp REP and subsequent modeling using transform theory found that it was necessary to include nonCondon effects to account for shifts in the maximum of the REP with respect to the maximum of the absorption spectrum (26). We observe that maxima of the modeled REP of some modes are shifted with respect to the experimental REP. Further, we also find that at shorter Raman excitation wavelengths, the simulated Raman profiles of some modes, for example, 1625 cm^{-1} (W1), 1556 cm^{-1} (W3), and 1360 cm^{-1} (W7), do not match experimental profiles. This is likely due to coupling of these modes to the higher electronic state (B_a) of Trp, which is close by and extends into the high frequency part of the B_b band. However, because we are using a global fit using a common set of parameters for all 14 observed modes, it is reasonable to expect that these effects will have a minor influence on the parameters determined for the B_b state.

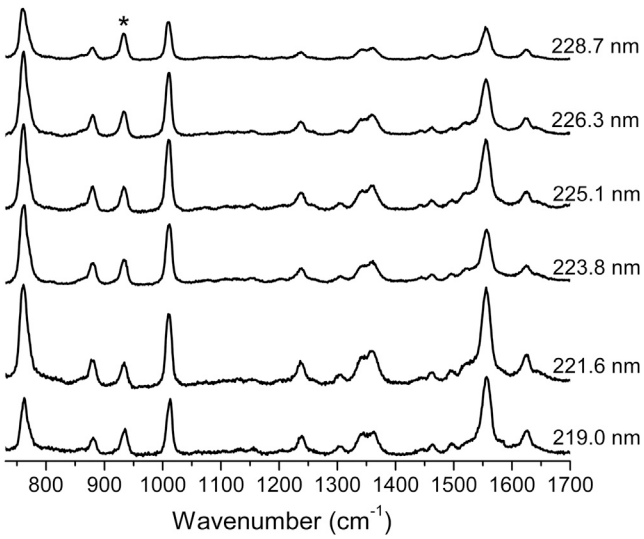

FIGURE 3 Resonance Raman spectra of tryptophan at six different excitation wavelengths. The spectra have been normalized to the intensity of the 932 cm^{-1} sodium perchlorate band (*asterisk*). Variation in the Raman spectrum as the excitation wavelength is tuned across the electronic absorption spectrum can be seen. Intensity of each spectrum is normalized to the intensity of the band of sodium perchlorate.

The intensity and position of the UVRR bands of Trp are known to be highly sensitive to differences in the local environment interactions. Changes in the relative intensity and frequency of the resonance Raman bands of a molecule are reflected in different contribution of the normal mode to the particular internal coordinate's changes, as can be seen from the Eq. 9. If there are large differences in the strength of the interactions of Trp with its local environments, then the structural changes upon optical excitation will be sensitive to these variations. The difference in the structure between the ground and excited state of Trp can also be susceptible to the normal mode composition changes, which are accounted for in the values of the coefficient A_{ij} in Eq. 9. Thus, it is possible to use the geometry change as a marker of the variations in the interactions of Trp in different local environments.

The displacements, Δ, corresponding to the best fit to the REP were used to compute the excited state structure in terms of the internal coordinates of the ground state. Raman cross-section depends on Δ^2 rather than Δ. As a consequence, the simulated REP values are insensitive to the sign of the displacement. However, this sign is important for computation of the excited state geometry in terms of internal coordinates of the molecule. To get around this ambiguity of the sign, we adopted the sign of the displacement according to the gradients previously reported by Jarzecki (31). In this work we have measured REPs of new bands in addition to those reported in previous work. For these new bands, the sign of delta was not available from previous calculations (31). These are low intensity modes with much smaller magnitude of the displacements along these normal modes than from other intense modes. Hence, contribution from these modes is not included in computation of the excited state geometry. These minor contributions do not affect conclusions about the qualitative changes in the ground state geometry upon photoexcitation but will alter their magnitude. Internal coordinates corresponding to the excited state are listed in Table 3.

The initial dynamics results in an overall expansion of the pyrrole ring together with a distortion of the benzene ring. Six modes, i.e., 1556 cm^{-1} (W3), 1360 cm^{-1} (W7),

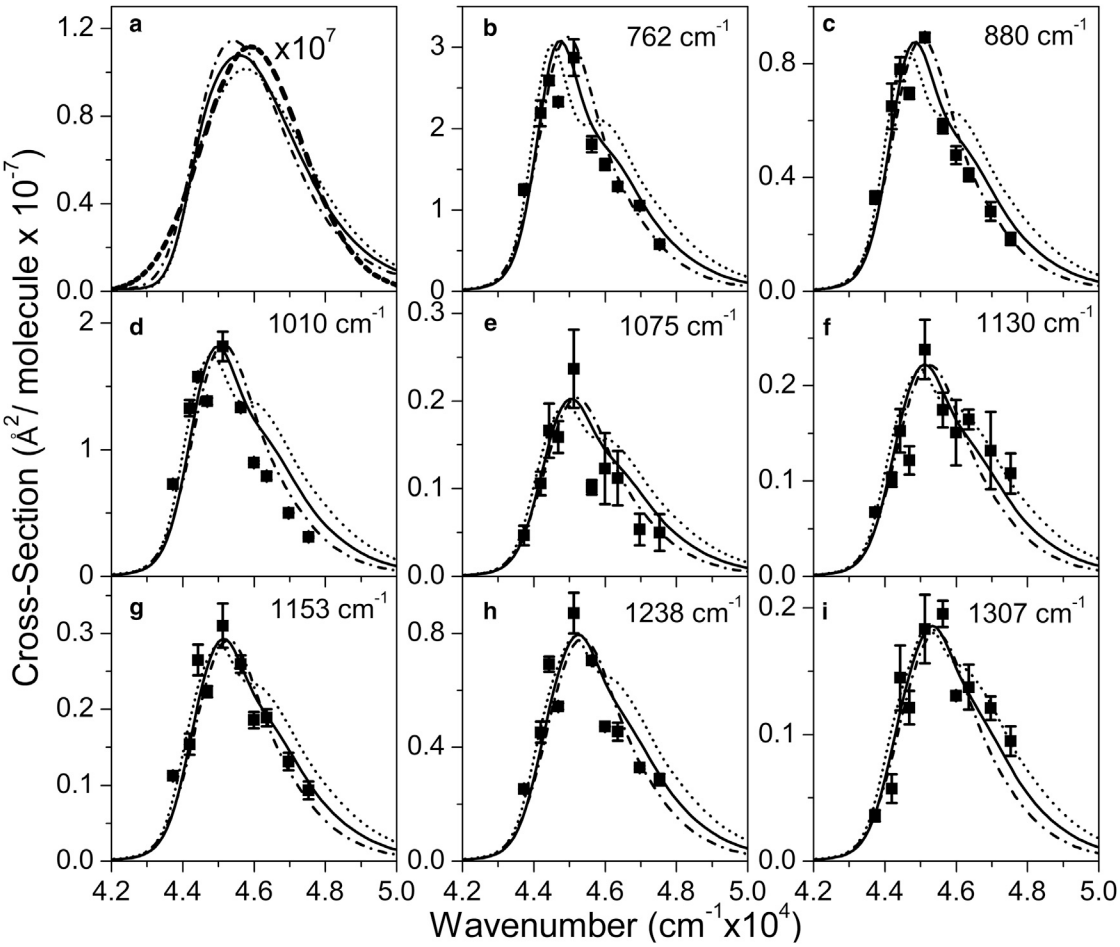

FIGURE 4 Experimental and simulated Raman excitation profiles and absorption cross-section for the B_b transition of tryptophan. (*a*) Experimental (*dashed*) and simulated (*solid*) absorption spectrum. (*b–i*) Experimental (*points*) and simulated (*solid*) Raman excitation profiles for eight resonant modes of tryptophan. The simulated absorption and Raman excitation profiles were obtained by using the parameters in Table 1. The best fit (*black*) was obtained using the dimensionless displacements in Table 2. Set 1 (*dash dot*) and Set 2 (*dot*) were obtained with two sets of deltas obtained by decreasing and increasing 20% those values in the best fit.

1238 cm^{-1} (W10), 1010 cm^{-1} (W16), 880 cm^{-1} (W17), and 762 cm^{-1} (W18), contribute to 83% of the total internal reorganization energy (λ_{int}). The total internal reorganization energy over these modes is 939 cm^{-1}. Consistent with the initial distortion of the ground state, the energy-minimized structure of the B_b state using DFT calculations also shows major changes in the Trp structure along the pyrrole ring and the benzene rings (29).

The changes in the structural geometry of Trp upon photoexcitation to the B_b excited state have been previously shown in two published reports by Gaff and Franzen (29) and Gaff et al. (30). In both cases, time-dependent DFT (TDDFT) calculations were used to determine the dimensionless displacements along the normal modes. The computed displacements were then used to determine the Raman cross-section by using theoretical expressions from the time-dependent wave packet theory and 3MI as a model of Trp. We will refer to the published work of Gaff and Franzen (29) and Gaff et al. (30) as the first and second reports, respectively. In the first report the calculated resonance Raman cross-sections of Trp at 218-nm excitation wavelength show in general good agreement with the experiment except for the W18 band (29). At 229-nm excitation wavelength, the agreement is better for the W18 band but major discrepancies occur in the other more intense bands of Trp. The second report shows a better agreement of the calculated relative cross-section of different bands (30).

The differences found between the two reports reflect the differences in the computed displacements, as can be seen in Table S4 that lists values of displacements obtained in the two reports and in our simulation. The differences are reflected in the calculated absolute and relative intensities of the bands of Trp. The application of a self-consistent procedure for the simulation of the experimental absorption and REP carried out in this work utilizes intensity measurements at several wavelengths to obtain the displacement. The excellent agreement of the simulated and experimental cross-sections, for all the modes at different excitation

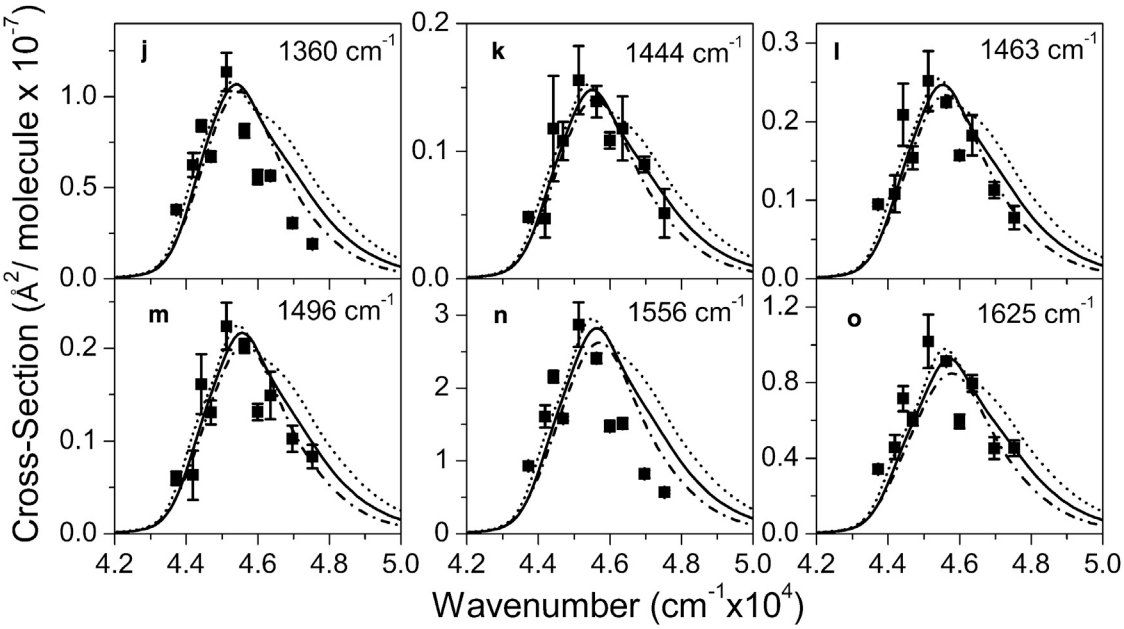

FIGURE 5 Experimental and simulated Raman excitation profiles of the other six resonant modes of tryptophan. The simulated Raman excitation profiles were obtained by using the same sets of parameters as in Fig. 4.

wavelengths, suggest that the values of displacements that we have obtained here better reflect the excited state geometry than those found by using TDDFT calculations.

Both the previous articles reported the changes in the internal coordinates (bond length) of Trp upon optical excitation. However, the predicted structural changes in the two reports are contradictory, as can be seen in Table S5 and no explanation for the differences was given in the second report. In the first report (see the Supporting Material), it was shown that there is expansion and contraction of several bonds (29); but in the second report, contraction was found in only one of the bonds (30). In the excited state structure computed with TDDFT in the second report (30), all the bonds in the indole ring experience expansion upon photoexcitation and a contraction in the C_1–C_{16} bond with respect to the ground state. Although our calculations also predict a contraction in the C_1–C_{16} bond, we find some differences between the predicted excited state geometry (30) and that determined from the calculations in this study. Major changes are found in the indole ring with expansion along most stretching coordinates of the ring bonds, but a contraction of C_3–C_5, C_5–C_7, and C_8–C_9 bonds. Ambiguity in the sign of displacement, Δ, used here as obtained by Jarzecki (31) and those of the second report of Gaff et al. (30) may partially account for the observed differences in the estimated structures.

The comparison with the computed structure of the first report shows better agreement with our predictions (29). Though the absolute and relative cross-sections have discrepancies with the experiment, the directions of the changes in bond length are in general similar to those we have found here. The major discrepancy in magnitude and sign occurs for the C_7=C_9 bond of benzene ring, which in our study shows small contraction, and in the first report of Gaff et al. (30) is one of the internal coordinates that suffers major expansion. The differences may occur due the different values of dimensionless displacements, as for example, those corresponding to the high intense W18 and W16 modes, which are known to have contribution from the benzene ring vibration. The difference between the changes of the C_1=C_2 bond length may also be due to different values of Δ of the W3 mode of Trp, which has major contribution from the C_1=C_2 stretching coordinate. An additional factor is that the dimensionless displacements are converted to internal coordinates by using force constants computed with DFT. Depending on the specific functional used and the basis set employed, the composition of the ground state normal modes can alter slightly, which is, in turn, reflected in the computed excited state geometry. Although there is some uncertainty in the excited state geometry, the mode-specific vibrational reorganization

TABLE 1 Parameters used in the simulations of the absorption and REP

	E_0 (cm^{-1})	Λ (cm^{-1})	τ (fs)	θ (cm^{-1})	M (Å)	λ_{int} (cm^{-1})	λ_S (cm^{-1})	λ (cm^{-1})
Best fit	45355	640	8.3	315	1.07	939	1230	2169
Set 1	45485	680	7.8	525	1.07	601	1250	1851
Set 2	45100	600	8.8	250	1.07	1352	1020	2372

TABLE 2 Normal mode experimental and calculated frequencies, dimensionless displacement, internal reorganization energy, and mode description for some modes of 3EI

Experimental frequencies (cm^{-1})	Calculated frequencies from 3EI (cm^{-1}) B3LYP/6-31G**	Potential energy distribution (%) from VEDA B3LYP/6-31G**	$\|\Delta\|$	Mode-specific internal reorganization energy (cm^{-1})
1556	1595	str C1C2 (44) be H10C2C1 (−11)	0.48	180.7
1360	1387	be C1C2N4 (10) be H14C8C9 (11)	0.32	71.4
1238	1269	be H10C2C1 (−11) tors H17C16C1C2 (16)	0.30	55.0
1010	1034	str C6C8 (11) str C7C9 (13) str C8C9 (37) be H12C6C3 (−12) be H13C7C9 (12)	0.52	135.9
880	887	be C6C8C9 (−24) be C5C7C9 (−17) be C8C9C7 (17) be C2N4C5 (17)	0.40	69.7
762	763	be C8C9C7 (10) be C2N4C5 (15)	0.83	263.7

energies obtained from these simulations are more reliable than the excited state displacements because they do not depend on the signs of mode displacements.

The second component of the reorganization energy, λ_s, corresponds to the response of the solvent (water) to an instantaneous change in the structure and charge distribution of the solute (tryptophan). Because Raman is a scattering phenomenon, and the exited state is not significantly populated, the solvent reorganization energy determined through Raman intensity analysis corresponds to the inertial response of water, which is known to occur in <100 fs (45,52,53). Contribution from the remaining components of the water relaxation response will be contained in the inhomogeneous broadening linewidth (θ) in our model. This inhomogeneous linewidth will also reflect the rotational dynamics of Trp in the picosecond-to-nanosecond timescale (5,54). Our simulations yield a dynamic solvent response of 8 fs from the water surrounding the Trp with solvent reorganization energy (λ_s) of 1230 cm^{-1}. We note, however, that the model is not sensitive to the timescale of dynamic solvent response. Effect of the solvent dynamical timescale on the overall REP fit is shown in Fig. S5, Fig. S6, and Table S6).

We compare the solvation characteristics measured by us with some of the previous reports in the literature. The solvation response of water has been extensively studied with several chromophores being used as probes (45,52). Experimental measurements of the timescale and amplitude of solvation responses have relied on fluorescence emission spectroscopy of solutes to measure dynamics of water. These experiments are limited in time-resolution because of the inherent nature of fluorescence emission processes that are preceded by internal relaxation. Nevertheless, some ultrafast studies have revealed the timescales of fast dynamics of water. Studies on coumarin showed that the solvation response of water is bimodal with an initial ultrafast component (55 fs) followed by a slower response (52). The local solvation dynamics of Trp in solution and in proteins has been examined by several theoretical and experimental studies at timescales ranging from femtoseconds to picoseconds. Ultrafast fluorescence spectroscopy and molecular dynamics simulations are especially popular methods of choice. Using femtosecond upconversion spectroscopy of Trp, the ultrafast response of water to excitation of Trp is found to have two components with characteristic times of 160–340 fs and 1–1.6 ps (5,7,9,10). These studies report on the solvent (or protein) response upon excitation of Trp to the L_a and L_b bands of Trp. Direct measurements of the solvation dynamics of Trp after excitation to the B_b band have not been done before. It is expected that the timescale of solvent response to excitation at L_a or L_b state versus the B_b states should be similar while the magnitude of the response will be dependent on the electronic distribution and consequent dipole moment of the solute. The mode-specific internal reorganization energy distribution will also be different as manifested in the differences of the resonance Raman spectra of Trp acquired in resonance with the two electronic states (24).

Molecular dynamics simulation of 3MI in water by Muino and Callis (6) predicts that water relaxation around a chromophore takes place with a fast inertial response in ~15 fs followed by an exponential decay of 400 fs corresponding to diffusive motions of the solvent. Recently, Bräm et al. (7) used molecular dynamics simulation to study the time-dependent emission spectra of the L_a band of Trp. Three components were found in the relaxation dynamics: 9 fs, 175 fs, and 1.2 ps. In contrast to these computational findings, no relaxation component with time decay below 100 fs has been explicitly detected experimentally for

TABLE 3 Changes in the internal coordinates for tryptophan along the indole ring (only those internal coordinates that suffer major changes)

Internal coordinates (Bond length)	Internal coordinates in ground state (Å)	Internal coordinates change (Å)
C_1=C_2	1.3765	0.03
C_1–C_3	1.4432	0.04
C_1–C_{16}	1.5039	−0.09
C_3=C_5	1.4271	−0.03
C_3–C_6	1.4081	0.07
N_4–C_5	1.3755	0.08
C_5–C_7	1.4013	−0.02
C_6=C_8	1.3905	0.03
C_8–C_9	1.4121	−0.09

solvation of Trp. The relaxation time obtained in this work (8 fs, corresponding to $\Lambda = 640 cm^{-1}$) is similar to that found by Bräm et al. (7) for the inertial response of water, faster than the time obtained by Muino and Callis (6) (15 fs), which corresponds to $\Lambda = 354\ cm^{-1}$. This implies that to have a 15-fs relaxation time in our calculation it is necessary to decrease the parameter Λ by approximately twofold. Attempt to use values in this range do not produce a good fit in the position of the REP and absorption spectrum simultaneously (shown in the Supporting Material). As mentioned earlier and noted by Cao and McHale (41) variations of Λ in the range of ~50 cm^{-1} do not produce major differences in the computed REP. Although the simulations do indicate that an ultrafast component of ~10 fs is present, the REP simulations cannot determine the timescale of this relaxation accurately.

To obtain an estimate of the total reorganization energy corresponding to solvation of Trp, it is necessary to include the contribution of processes occurring at timescales longer than 100 fs, e.g., interconversion between the rotational isomers of Trp. These processes would contribute to the inhomogeneous broadening linewidth (315 cm^{-1}) in our experiments and simulations. Bräm et al. (7) and Lu et al. (12) estimated the contribution of rotamer dynamics to the total Stokes shift due to solvation dynamics at 200 cm^{-1}. After removing a contribution of 100 cm^{-1}(2 × reorganization energy = Stokes shift) from the dynamics of indole rotamers, the contribution of slower solvation processes to the inhomogeneous broadening, θ_s, is estimated as (315–100 = 215 cm^{-1}). The total solvent reorganization energy of Trp at timescales longer than 100 fs is estimated at ($\theta_s + \lambda_s$) = 1445 cm^{-1}. Thus, the inertial component contributes 85% to the total solvent response.

The inertial component of the response obtained by Bräm et al. (7) contributes 1700 cm^{-1} to the Stokes shift (7), which corresponds to solvent reorganization energy of 850 cm^{-1}. Muino and Callis (6) also found that the initial solvent response to the excitation of 3MI contributes 50% (2000 cm^{-1}) to the total Stokes shift (6). Thus, 1000 cm^{-1} of the solvent reorganization energy can be estimated from the Stokes shift. These values are lower than the values we have obtained in this work. We note that the solvent dynamics based on the Stokes shift has contribution only from the solvent response and no contribution from the internal reorganization energy of the solute. The internal reorganization energy associated with excitation of Trp to the B_b band makes a significant contribution of 43% to the total reorganization energy (2169 cm^{-1}). Thus, the internal reorganization energy of Trp in the B_b state will play an important role in its excited state dynamics and must be taken into account. The higher values of solvent reorganization energy in our studies in comparison with those obtained by excitation to the L_a suggests a greater amplitude of response of the solvent due to the larger dipole moment of the structure of Trp in the B_b excited state (55).

It is known that a different set of parameters can fit the absorption and REP simultaneously, and it is required to determine the limits of variability of parameters that produce good fit. For that we have used two sets of deltas obtained by decreasing and increasing 20% those values in the best fit. At each set of values for the displacements, the values of 0-0 energy, the lineshape function, and the inhomogeneous broadening linewidth were optimized through a least-squares fit. For the set of smaller deltas (Set 1), it was possible to get an adequate fit of the Raman intensity but not in the position of the absorption spectrum (Figs. 4 and 5). A value of 1250 cm^{-1} of the solvent reorganization energy was required, which is closer to the value obtained for the best fit. However, the value of the inhomogeneous broadening linewidth had to be increased to 525 cm^{-1} (Table 1). For the higher values of deltas (Set 2), it was not possible to get a good fit of both the absorption and REP shape. Decrease in the values of the solvent reorganization energy (1020 cm^{-1}) and inhomogeneous broadening linewidth (250 cm^{-1}) was required to improve the quality of the fit. From this analysis we can assume limits of variability of the solvent reorganization energy from 1020 cm^{-1} to 1250 cm^{-1} and 250 cm^{-1} to 525 cm^{-1} for the inhomogeneous broadening linewidth. However, simultaneous fit to the absorption and the REP constrained the range of variability to allow the choice of the parameters corresponding to the best fit. We note that because this work analyzes Raman intensities through modeling of the lineshape, the results are dependent on the choice of the model used. We chose the simplest possible model that can partition the overall broadening into inhomogeneous and homogeneous component.

CONCLUSION

Protein dynamics and hydration are now taking the center stage in the evolving paradigm of protein function. Trp has been an informative intrinsic chromophore in furthering the understanding of these aspects of proteins. Several studies have used Trp as a probe of hydration and protein dynamics (9–14). These studies have revealed that Trp dynamics range from femtoseconds to hundreds of picoseconds. However, delineating the mechanistic origin of observed dynamics at various timescales is a challenge. Further work is required to identify the processes responsible for the dynamics at different timescales and evaluate the precise role of water in these relaxation processes. In this work we extracted ultrafast solvent response to photoexcitation of Trp from simulation of the Raman excitation profiles, which shows that there is a <50 fs component in the dynamics of free tryptophan. Put together, these and previous studies show that the dynamics of tryptophan is complex, with processes at various timescales and warrants further investigation. These data also impact studies on proteins that utilize Trp as a probe of protein dynamics.

We found that the inertial response of the solvent contributes to 85% of the estimated total solvent response (1445 cm^{-1}). The improved fits to the Raman line-shapes of Trp obtained here with the Mukamel model show that it is essential to incorporate solvent response. The structure of the excited state of Trp determined through Raman intensities shows that there is extensive distortion of the Trp ring. Thus UV photoexcitation of tryptophan will lead to significant charge redistribution. These effects are expected to persist in the protein environment although the relative magnitudes will be modulated. We are now extending these experiments and analysis to employ a tryptophan residue buried inside a protein as a probe of the local protein response.

SUPPORTING MATERIAL

Six figures and six tables are available at http://www.biophysj.org/biophysj/supplemental/S0006-3495(13)00512-2.

We thank Rajaram Nityananda for valuable discussions and for critical reading of the manuscript.

REFERENCES

1. Demchenko, A. P. 1986. Ultraviolet Spectroscopy of Proteins. Springer, New York.
2. Lakowicz, J. R. 2006. Principles of Fluorescence Spectroscopy. Springer, New York.
3. Schauerte, J. A., D. G. Steel, and A. Gafni. 1997. Time-resolved room temperature tryptophan phosphorescence in proteins. *Methods Enzymol.* 278:49–71.
4. Balakrishnan, G., C. L. Weeks, …, T. G. Spiro. 2008. Protein dynamics from time resolved UV Raman spectroscopy. *Curr. Opin. Struct. Biol.* 18:623–629.
5. Shen, X. H., and J. R. Knutson. 2001. Subpicosecond fluorescence spectra of tryptophan in water. *J. Phys. Chem. B.* 105:6260–6265.
6. Muino, P. L., and P. R. Callis. 1994. Hybrid simulations of solvation effects on electronic spectra: indoles in water. *J. Chem. Phys.* 100:4093–4109.
7. Bräm, O., A. A. Oskouei, …, M. Chergui. 2010. Relaxation dynamics of tryptophan in water: a UV fluorescence up-conversion and molecular dynamics study. *J. Phys. Chem. A.* 114:9034–9042.
8. Toptygin, D., T. B. Woolf, and L. Brand. 2010. Picosecond protein dynamics: the origin of the time-dependent spectral shift in the fluorescence of the single Trp in the protein GB1. *J. Phys. Chem. B.* 114:11323–11337.
9. Zhong, D. P., S. K. Pal, …, A. H. Zewail. 2002. Femtosecond dynamics of rubredoxin: tryptophan solvation and resonance energy transfer in the protein. *Proc. Natl. Acad. Sci. USA.* 99:13–18.
10. Pal, S. K., J. Peon, and A. H. Zewail. 2002. Biological water at the protein surface: dynamical solvation probed directly with femtosecond resolution. *Proc. Natl. Acad. Sci. USA.* 99:1763–1768.
11. Peon, J., S. K. Pal, and A. H. Zewail. 2002. Hydration at the surface of the protein Monellin: dynamics with femtosecond resolution. *Proc. Natl. Acad. Sci. USA.* 99:10964–10969.
12. Lu, W. Y., J. Kim, …, D. P. Zhong. 2004. Femtosecond studies of tryptophan solvation: correlation function and water dynamics at lipid surfaces. *Chem. Phys. Lett.* 388:120–126.
13. Zhang, L. Y., Y. T. Kao, …, D. Zhong. 2006. Femtosecond studies of tryptophan fluorescence dynamics in proteins: local solvation and electronic quenching. *J. Phys. Chem. B.* 110:18097–18103.
14. Qiu, W. H., L. J. Wang, …, D. Zhong. 2007. Dissection of complex protein dynamics in human thioredoxin. *Proc. Natl. Acad. Sci. USA.* 104:5366–5371.
15. Uversky, V. N., and E. A. Permyakov. 2007. Methods in Protein Structure and Stability Analysis: Luminescence Spectroscopy and Circular Dichroism. Nova Science Publishers, New York.
16. Austin, J. C., T. Jordan, and T. G. Spiro. 1993. Ultraviolet resonance Raman studies of proteins and related model compounds. *In* Biomolecular Spectroscopy. John Wiley, New York.
17. Asher, S. A. 1988. UV resonance Raman studies of molecular structure and dynamics: applications in physical and biophysical chemistry. *Annu. Rev. Phys. Chem.* 39:537–588.
18. Takeuchi, H. 2003. Raman structural markers of tryptophan and histidine side chains in proteins. *Biopolymers.* 72:305–317.
19. Thomas, Jr., G. J. 1999. Raman spectroscopy of protein and nucleic acid assemblies. *Annu. Rev. Biophys. Biomol. Struct.* 28:1–27.
20. Myers, A. B. 1990. Femtosecond molecular dynamics probed through resonance Raman intensities. *J. Opt. Soc. Am. B.* 7:1665–1672.
21. Myers, A. B. 1997. 'Time-dependent' resonance Raman theory. *J. Raman Spectrosc.* 28:389–401.
22. Myers Kelley, A. 2008. Resonance Raman and resonance hyper-Raman intensities: structure and dynamics of molecular excited states in solution. *J. Phys. Chem. A.* 112:11975–11991.
23. Stuart, C. M., R. R. Frontiera, and R. A. Mathies. 2007. Excited-state structure and dynamics of *cis*- and *trans*-Azobenzene from resonance Raman intensity analysis. *J. Phys. Chem. A.* 111:12072–12080.
24. Asher, S. A., M. Ludwig, and C. R. Johnson. 1986. UV resonance Raman excitation profiles of the aromatic amino acids. *J. Am. Chem. Soc.* 108:3186–3197.
25. Fodor, S. P. A., R. A. Copeland, …, T. G. Spiro. 1989. Deep-ultraviolet Raman excitation profiles and vibronic scattering mechanisms of phenylalanine, tyrosine, and tryptophan. *J. Am. Chem. Soc.* 111:5509–5518.
26. Sweeney, J. A., and S. A. Asher. 1990. Tryptophan UV resonance Raman excitation profiles. *J. Phys. Chem.* 94:4784–4791.
27. Chang, S., W. Yang, and T. G. Spiro. 1990. Saturation effects on ultraviolet resonance Raman intensities: excimer/YAG laser comparison and aromatic amino acid cross-sections. *J. Raman Spectrosc.* 21:435–440.
28. Marconi, G. 1991. Theoretical analysis of the resonance Raman spectrum of tryptophan. *J. Raman Spectrosc.* 22:361–365.
29. Gaff, J. F., and S. Franzen. 2009. Excited-state geometry method for calculation of the absolute resonance Raman cross sections of the aromatic amino acids. *J. Phys. Chem. A.* 113:5414–5422.
30. Gaff, J. F., S. Franzen, and B. Delley. 2010. Ab initio calculation of resonance Raman cross sections based on excited state geometry optimization. *J. Phys. Chem. A.* 114:11681–11690.
31. Jarzecki, A. A. 2009. Quantum-mechanical calculations of resonance Raman intensities: the weighted-gradient approximation. *J. Phys. Chem. A.* 113:2926–2934.
32. Lee, S. Y., and E. J. Heller. 1979. Time-dependent theory of Raman scattering. *J. Chem. Phys.* 71:4777–4788.
33. Li, B. L., A. E. Johnson, …, A. B. Myers. 1994. The Brownian oscillator model for solvation effects in spontaneous light emission and their relationship to electron transfer. *J. Am. Chem. Soc.* 116:11039–11047.
34. Mukamel, S. 1995. Principles of Nonlinear Optical Spectroscopy. Oxford University Press, New York.
35. DeVito, V. L., M. Z. Cai, …, K. M. Smith. 1992. UV resonance Raman evidence for electronically and vibrationally independent protoporphyrin IX vinyl groups. *J. Phys. Chem.* 96:6917–6922.

36. Dudik, J. M., C. R. Johnson, and S. A. Asher. 1985. Wavelength dependence of the preresonance Raman cross-sections of CH_3CN, SO^{2-}_4, $C1O^{-}_4$, and NO^{-}_3. *J. Chem. Phys.* 82:1732–1740.

37. Myers, A. B. 1995. Excited Electronic State Properties from Ground State Resonance Raman Intensities. Wiley, New York.

38. Myers, A. B., and R. A. Mathies. 1987. Resonance Raman intensities: a probe of excited state structure and dynamics. *In* Biochemical Applications of Raman Spectroscopy. Wiley, New York.

39. Puranik, M., S. Umapathy, …, J. Chandrasekhar. 2001. Structure of the triplet excited state of bromanil from time-resolved resonance Raman spectra and simulation. *J. Chem. Phys.* 115:6106–6114.

40. Zhao, X. H., J. A. Burt, and J. L. McHale. 2004. Resonance Raman analysis of nonlinear solvent dynamics: betaine-30 in ethanol. *J. Chem. Phys.* 121:11195–11201.

41. Cao, X., and J. L. McHale. 1998. Resonance Raman study of solvent dynamics on the spectral broadening and intramolecular charge transfer of a hemicyanine dye in aqueous solution. *J. Chem. Phys.* 109:1901–1911.

42. Moran, A. M., and A. M. Kelley. 2001. Solvent effects on ground and excited electronic state structures of p-nitroaniline. *J. Chem. Phys.* 115:912–924.

43. Waterland, M. R., S. L. Howell, and K. C. Gordon. 2007. Using internal coordinates to describe photoinduced geometry changes in MLCT excited states. *J. Phys. Chem. A.* 111:4604–4611.

44. Loppnow, G. R., and R. A. Mathies. 1988. Excited-state structure and isomerization dynamics of the retinal chromophore in rhodopsin from resonance Raman intensities. *Biophys. J.* 54:35–43.

45. Jimenez, R., D. A. Case, and F. E. Romesberg. 2002. Flexibility of an antibody binding site measured with photon echo spectroscopy. *J. Phys. Chem. B.* 106:1090–1103.

46. Frisch, M. J., G. W. Trucks, …, J. A. Pople. 2003. Gaussian 03, Rev. E.01. Gaussian, Pittsburgh, PA.

47. Becke, A. D. 1993. Density-functional thermochemistry. III. The role of exact exchange. *J. Chem. Phys.* 98:5648–5652.

48. Lee, C. T., W. T. Yang, and R. G. Parr. 1988. Development of the Colle-Salvetti correlation-energy formula into a functional of the electron density. *Phys. Rev. B Condens. Matter.* 37:785–789.

49. Takeuchi, H., and I. Harada. 1986. Normal coordinate analysis of the indole ring. *Spectrochim. Acta A Mol. Biomol. Spectrosc.* 42:1069–1078.

50. Harada, I., T. Miura, and H. Takeuchi. 1986. Origin of the doublet at 1360 and 1340 cm^{-1} in the Raman spectra of tryptophan and related compounds. *Spectrochim. Acta A Mol. Biomol. Spectrosc.* 42:1069–1078.

51. Dieng, S. D., and J. P. M. Schelvis. 2010. Analysis of measured and calculated Raman spectra of indole, 3-methylindole, and tryptophan on the basis of observed and predicted isotope shifts. *J. Phys. Chem. A.* 114:10897–10905.

52. Jimenez, R., G. R. Fleming, …, M. Maroncelli. 1994. Femtosecond solvation dynamics of water. *Nature.* 369:471–473.

53. Lang, M. J., X. J. Jordanides, …, G. R. Fleming. 1999. Aqueous solvation dynamics studied by photon echo spectroscopy. *J. Chem. Phys.* 110:5884–5892.

54. Beechem, J. M., and L. Brand. 1985. Time-resolved fluorescence of proteins. *Annu. Rev. Biochem.* 54:43–71.

55. Chi, Z. H., and S. A. Asher. 1998. UV Raman determination of the environment and solvent exposure of Tyr and Trp residues. *J. Phys. Chem. B.* 102:9595–9602.